Chem. Res. Chin. Univ., 2016, 32(1), 76—81 doi: 10.1007/s40242-016-5345-x

Amorphous Structure and Bonding Chemistry of Aluminium Antimonide(AlSb) Alloy for Phase-change Memory Device

SUN Yu[1], WANG Xuepeng[1*], DU Jiaren[1], CHEN Nianke[1], YU Hongmei[2*], WU Qi[2] and MENG Xing[3]

1. State Key Laboratory on Integrated Optoelectronics, College of Electronic Science and Engineering, 2. College of Computer Science and Technology, 3. College of Physics, Jilin University, Changchun 130012, P. R. China

Abstract With the help of first-principles molecular dynamics calculations, we obtained the atomic picture of amorphous AlSb(a-AlSb) for phase-change memory application. Generally, a-AlSb shows sp^3 bonding network, which is the intrinsic characteristic for its good thermal stability. Significant wrong(homogenous) Al-Al bonds can also be observed from the pair correlation function. This hints the amorphous phase may consist of Al cluster and Sb-rich Al-Sb alloy. Recent experiment has observed the Sb-rich region of AlSb alloy can be switched to crystal, on the basis of which, combined with our calculations, we thus propose that on the one hand such a Sb-rich region in a-AlSb can retain the rapid crystallization like pure Sb solid and on the other hand some Al atoms play the important role of stabilizing Sb rich network with sp^3 bonding. The present study offers a microscopic view to understand the phase change mechanism of AlSb alloy for information storage device.

Keywords AlSb alloy; Amorphous phase; Phase-change memory device; *Ab initio* calculation

1 Introduction

Phase-change materials show very fast phase transition between amorphous and crystalline phase, while the two phases keep significant electrical/optical contrast[1,2]. Thus, they can be used in fast and nonvolatile phase-change memory(PCM). As early as 1968, Ovshinsky[3] discovered this phenomenon. In fact, this memory technology has been recognized as an important candidate for the next generation nonvolatile memory[4,5]. The PCM materials mainly include chalcogenides, such as In_3SbTe_2, TiSbTe, SiSbTe and GeSbTe[6—9]. Among them, $Ge_2Sb_2Te_5$(GST) has been most widely studied and employed due to its excellent properties[10]. It has been used in Blue-ray DVD[11,12]. However, GST holds a relative low crystallization temperature(430 K)[13], which has limited its application in, such as, automobile industry.

Moreover, Te easily diffuses and separates at a high temperature because of its low melting point. Meanwhile, Te is also an overly active element in PCM materials[14]. In 2003, van Pieterson *et al.*[15] presented Te-free Sb based phase-change materials that exhibit fast crystallization with excellent stability of amorphous phase at room temperature. Generally, Sb easy crystallizes, so the stability of its amorphous phase is poor. When Sb was doped with other elements, such as Ge and Si[16,17], new kinds of PCM materials have been proposed with a good stability of amorphous phase. AlSb is one of these Sb based PCM materials. According to the work of Zhou *et al.*[18], AlSb with a composition ratio of 1:1 showed relatively high crystallization temperature(482 K), which was reflected by a 10-year data retention temperature of 376 K. This indicates AlSb is also an important candidate for future nonvolatile PCM. Meanwhile, at a low resistance state of AlSb(crystalline AlSb, c-AlSb), only the indication of A7-type structure can be found in XRD and selected area electron diffraction(SAED) patterns, which indicates c-AlSb must have a very significant Sb rich region. In other words, a certain degree of phase separation may occur during amorphous-crystalline transition. Therefore, to get the amorphous picture of AlSb is the first step to understand the chemical bonding tendency and thus the switch mechanism.

Ab initio molecular dynamics(AIMD) has been widely used to explore the atomic structure and mechanism of fast phase transition of PCM materials[19—21]. In this work, we will try to analyze the local atomic picture of amorphous AlSb (a-AlSb) and shed light on possible switching mechanism of AlSb by AIMD method. Analyzing its bond angle distribution and coordination number, we demonstrated that the atomic configuration in a-AlSb is mainly sp^3 bonding network which reflects its intrinsic thermal stability in contrast to that of *p*-orbital resonant bonding in crystal state[22]. Significant Al-Al

*Corresponding authors. E-mail: wangxpjlu@foxmail.com; hmyu@jlu.edu.cn

Received September 2, 2015; accepted September 28, 2015.

Supported by the China Postdoctoral Science Foundation(No.2013T60315) and the National Natural Science Foundation of China(No.11374119).

wrong bonds indicate it also has a certain degree of phase separation in its amorphous phase. Electronic bonding characteristics are reflected by electron localization function(ELF) and charge density differences (CDD). Both ELF and CDD analyses further demonstrate that the covalent bonding of Al-Sb is dominated. In a-AlSb many of the Al-Al bonds keep metallic while some of those display interesting covalent characteristic. In other words, a-AlSb can have Sb-rich region. We proposed that on the one hand such a Sb-rich region in amorphous AlSb can retain the rapid crystallization like pure Sb solid and on the other hand Al atoms can stabilize the Sb-rich network through sp^3 bonding. Therefore, the present study offers a local atomic picture to understand the switching mechanism of AlSb alloy for PCM.

2 Computational Methods

Our calculation employed density functional theory (DFT)[23,24] was implemented in the Vienna *ab initio* Simulation Package(VASP) code[25,26]. The projector augmented wave(PAW) pseudopotential[27,28] was used to describe the electron-ion interaction, and the electronic exchange-correlation interaction was described by generalized gradient approximation(GGA)[29] with the Perdew-Burke-Ernzerhof (PBE) functional[30]. In AIMD simulation, we used the NVT canonical ensemble, in which the Nosé-Hoover thermostat was used to control the temperature. Melt-quenching amorphization method was used to obtain the model of a-AlSb. Our model contained 128 atoms with a density of 35.3 atoms/nm^3 according to ref.[31]. The initial model was firstly melt at 3000 K for 9 ps in order to eliminate the setup memory, and then was quenched down to 1400 K, a little higher than the melting point(1333 K[32]) of crystal AlSb, at which it was maintained for 9 ps to obtain stable liquid phase. Finally, we maintained the constant temperature set at 300 K for 15 ps to rapidly solidify the former liquid phase and obtain the a-AlSb atomic structure, see Fig.1(A). Time step for each AIMD was 3 fs, and the last 3 ps(1000 steps) was used to analyze the structural properties of a-AlSb. Electronic properties analysis was based on the final structure after geometry optimization.

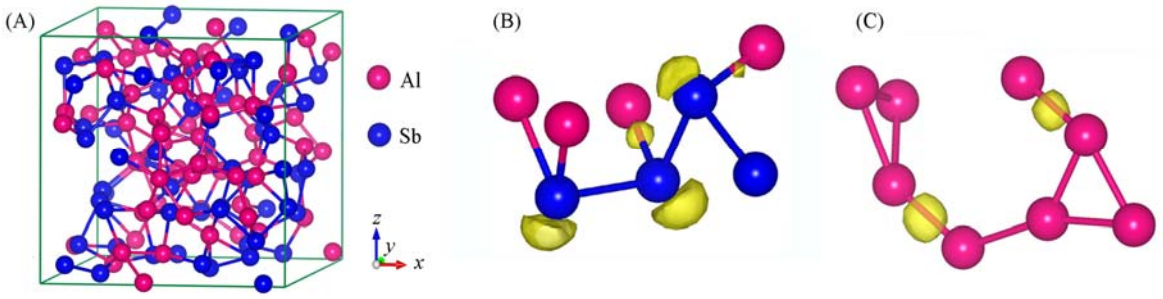

Fig.1 Final atomic structure of amorphous AlSb model at 300 K(A) and typical motifs of Sb(B) and Al(C) with high localized electrons distribution(cap like areas, ELF >0.9)

3 Results and Discussion

As a prerequisite, we must insure atoms during the AIMD procedure at high temperatures have already sufficiently diffused, so that a-AlSb model is not affected by the initial setup. We firstly calculated the mean square displacement(MSD) of two AIMD processes at 3000 and 1400 K. Fig.2(A) and (B) display a nearly linear increasing tendency of MSD for the total atoms and individual element ones. The slope of MSD is proportional to the diffusion coefficient. Obviously, Al has a larger diffusion coefficient than Sb due to the lighter atomic mass. This indicates Al is more active in the liquid. It is well known that amorphous phase is lack of long-range order, so we calculated the pair correlation function(PCF) of the final a-AlSb model at 300 K. As shown in Fig.2(C), for PCFs of different element pairs, our a-AlSb model was proved to be completely disorder due to the convergence of 1 at r>0.8 nm. Besides for the normal Al-Sb bonding, we can also observe the significant Al-Al bonding in the amorphous phase, which may be linked to the accumulation of Al. Finally, we checked optical properties contrast by calculating imaginary part of the dielectric function(ε_2). The dielectric function calculation was performed by the Cambridge Sequential Total Energy Package(CASTEP) program as implemented in the Materials Studio software. The frequency range may be lower than the experiment result, which is due to the band gap underestimate of DFT calculations[33]. As shown in Fig.2(D), the distribution of ε_2 for a-AlSb can be divided into three parts. In a range of 0—1 eV, the large ε_2 is mainly ascribed to dangling bonds and Al 3-fold rings(Drude model) which will be mentioned later. We can also see contrast between a-AlSb and c-Sb in a range of 1 to 2 eV. While in the scope of >2 eV, the ε_2 of a-AlSb resembles that of zinc blend AlSb(z-AlSb). Because there are a large amount of Al-Sb covalent bonds in both of them(this will also confirmed later).

Next, bond structure analysis was based on the a-AlSb model. First, we calculated bond angle distribution(BAD) and coordination number(CN) distribution. The BAD and CN distribution are closely related to bond length cutoff. The bond length cutoff is usually chosen according to the covalent radius[34], PCFs or ELF[35]. We chose 1.15 times the covalent radius as bond length cutoff, *i.e.*, 0.2898, 0.3059 and 0.322 nm for Al-Al, Al-Sb and Sb-Sb bond connections, respectively. The results were averaged for the last 3 ps(1000 steps) at 300 K. Fig.3(A) and (B) show the BAD and CN distribution, respectively. Most of Al and Sb still hold the BAD close to 109.5° and the max CN of 4. This distribution strongly indicates the main network around Al or Sb is sp^3 bonding type. Besides the

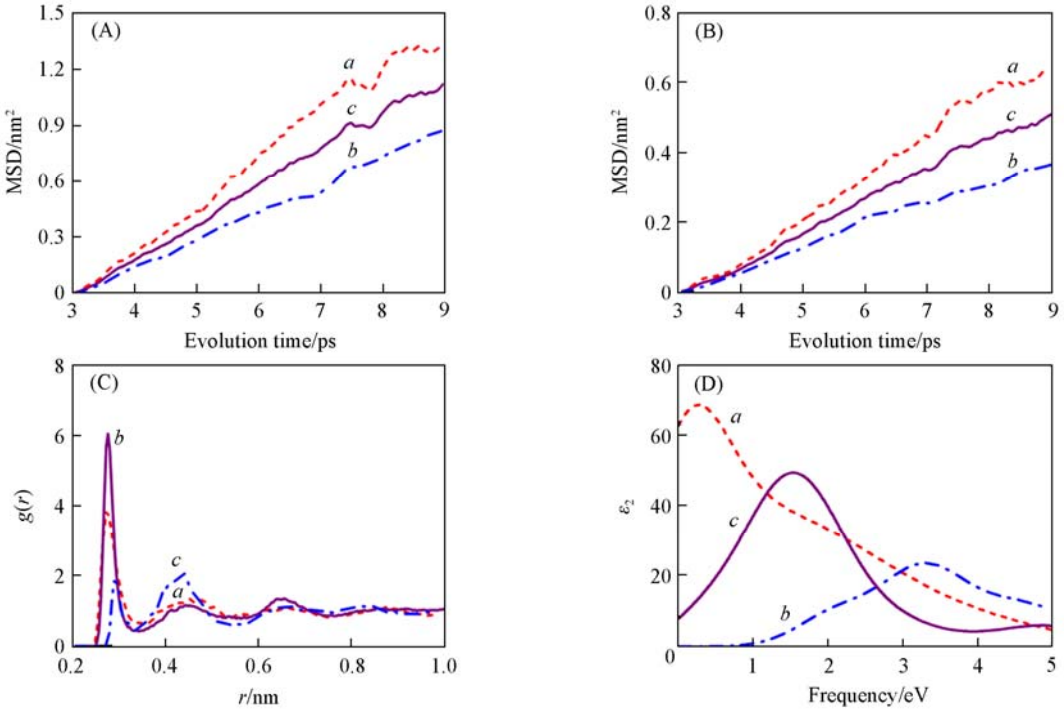

Fig.2 Mean square displacement(MSD) of Al(*a*), Sb(*b*) and all the atoms(*c*) at AIMD of 3000 K(A) and 1400 K(B), pair correlation function(PCF) for different element pairs[Al-Al(*a*), Al-Sb(*b*) and Sb-Sb(*c*)] in a-AlSb at 300 K(C) and imaginary part of the dielectric function(ε_2) for amorphous AlSb(*a*), zinc blend AlSb(*b*) and crystal Sb(*c*)(D)

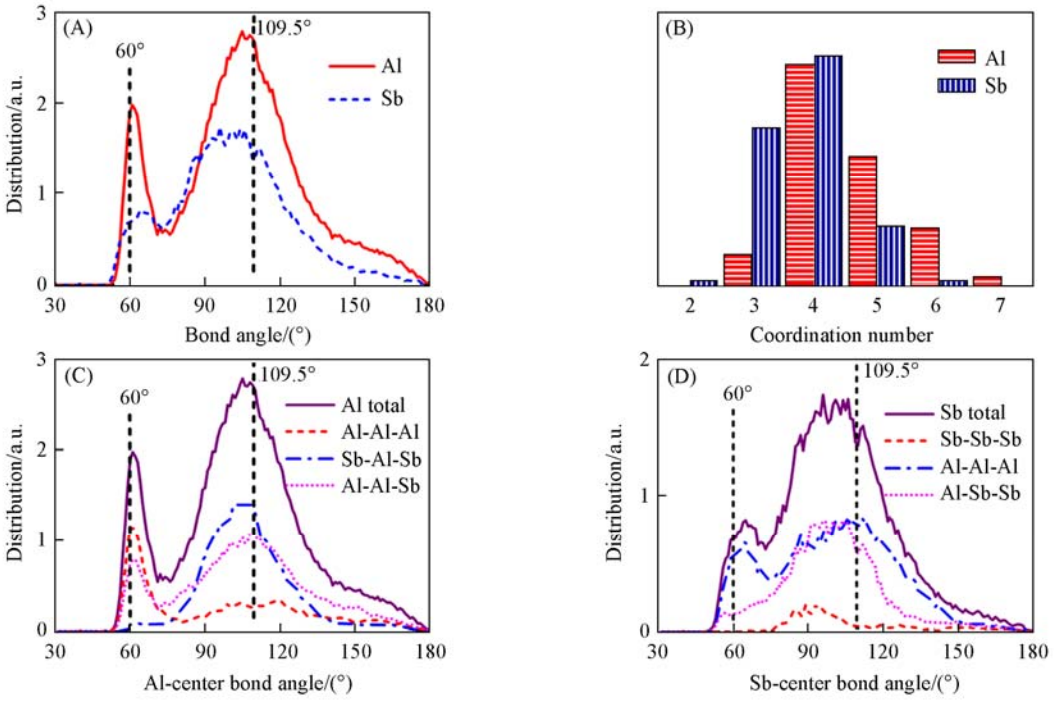

Fig.3 BAD(A) and CN distribution(B) of all the Al and Sb atoms, and BAD for different element pairs centered at Al(C) and Sb(D), respectively

case mentioned above, a significant BAD around 60° can be also observed for Al, which indicates a part of Al atoms may form 3-fold-ring structure in the present amorphous model.

In order to find the origin of 3-fold rings for the BAD around 60°, we divided the BAD into one part centered at Al and the other part centered at Sb. Fig.3(C) and (D) show the results. Obviously, the main contribution of 60° bond angle for Al comes from Al-Al-Al and Al-Al-Sb local connections, which strongly indicates the bonding tendency might have been changed to metallic characteristic when Al atoms got together. This is also demonstrated by the weakening of BAD around

109.5° for Al-Al-Al connection. Bond geometry of Al is quite similar to that of Ga in GaSb phase change material[36]. Yet, the heterogeneous connections of Sb-Al-Sb still maintain the BAD around 109.5°. Interestingly, a very small part of Sb-Sb-Sb local connections can be observed. The Sb homopolar connections have a bond angle distribution around 90°, which is the sign of *p*-bonding characteristics. Then we calculated the average total and partial coordination numbers. The total CN of Al and that of Sb are 4.54 and 3.78, respectively. For Al, the CN of Al-Al is 1.77, and the CN of Al-Sb is 2.78. For Sb, the CN of Sb-Sb is 1.01, and the CN of Sb-Al is 2.77. According to the results, we can get two conclusions. First, Sb exhibits a total average CN around 4 because of its main sp^3 type network. Al shows a relatively large average CN of 4.54 which reflects its significant Al-Al connection with possible additional metallic property. Second, the CN of Al-Al accounts for about 40% of the Al total CN. So it means that Al tends to get together and form clusters, which may lead to a nanoscale phase separation of a-AlSb. In order to inspect this, we calculated the fractions of Al and Sb atoms that bond to various elements in a-AlSb during the final AIMD process at 300 K, the results are shown in Table 1. Obviously, about 2.25% of Al atoms bond to Al only. In contrast, the ratio of Sb bonding only with Sb is much smaller(0.05%). This further supports a small part of Al has gotten together in a-AlSb model.

Table 1 Fractions of Al and Sb atoms bonding to various elements in a-AlSb model at 300 K

Atom	Fraction(%)		
	Al	Al and Sb	Sb
Al	2.25	72.10	25.65
Sb	29.46	70.49	0.05

In sum, the present a-AlSb model shows a main form of sp^3 heterogeneous connection. Meanwhile, Al metallic homopolar connection also exists. The present bond structure analysis results demonstrate that the main network of a-AlSb retains sp^3 type structure. A small part of Al tends to get together which is demonstrated by the BAD around 60° and the significant peak of Al-Al PCF. According to the observed phenomena of experiment[18], crystallization process mainly happens in the Sb-rich region. After a part of Al accumulation during amorphization, Sb-rich region may play the important role in the phase transition.

Finally, the electronic structure of the a-AlSb model was presented. We firstly calculated the electronic local function(ELF)[37]. ELF can be described in the form of a contour plot in the real space with values ranging from 0 to 1. The approaching region with ELF close to 1 indicates the strong covalent electrons or lone-pair electrons, the region with ELF close to 0 is typical for a low electron density area, and the region with ELF close to 0.5 is an area with homogenous electron gas. Fig.1(B) and (C) respectively show typical motifs of Sb and Al with high localized electrons(ELF>0.9) distribution in a-AlSb model. Most of such electrons locate at "cap" around Sb atoms with a CN of 3, which reflects the lone-pair of electrons in Sb. More interestingly, there are also high localization electrons between two Al atoms, which indicates their strong covalent bond characteristic. Fig.4 plots the typical ELF distribution through some slices, which are defined by some three-atom planes. For the slices of Al-Al-Al 3-fold ring and Al-Sb-Al 3-fold ring in Fig.4(A) and (B), Al-Al connection displays an ELF of *ca*. 0.5, which indicates the metallic characteristic of these 3-fold rings. For the slices of Al-Sb-Al, Sb-Al-Sb and Sb-Al-Al in Fig.4(C)—(E), respectively, the ELF(along Sb to Al) is about 0.8—0.9, which clearly indicates their covalent characteristic. However, in Fig.4(F), another Al-Al connection shows an ELF of *ca*. 0.8, which indicates the interesting covalent bonding again.

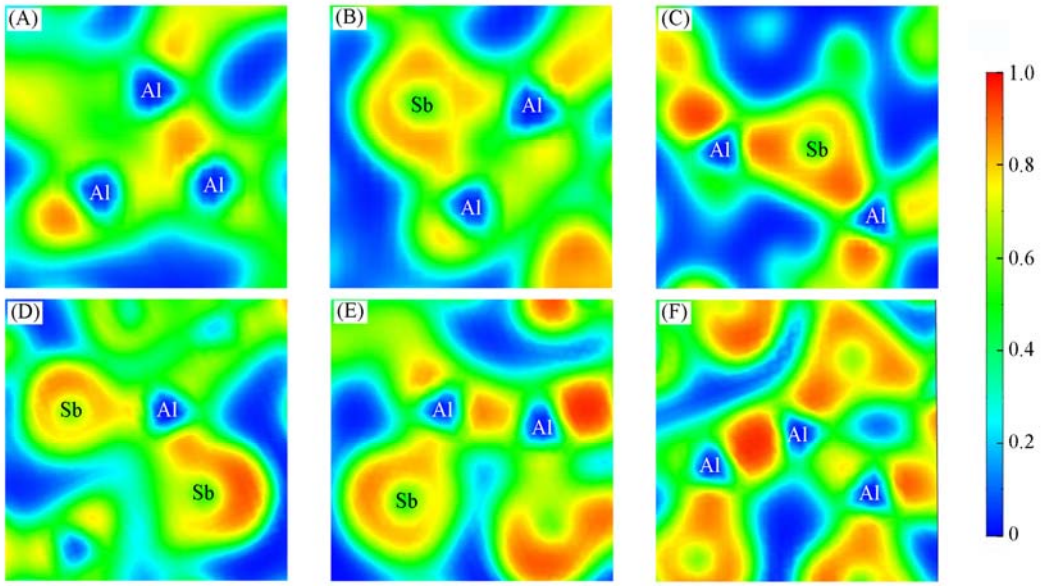

Fig.4 Typical bonding through the slice of ELF defined by the following three-atom planes

(A) Al-Al-Al ring; (B) Al-Sb-Al ring; (C) Al-Sb-Al plane; (D) Sb-Al-Sb plane; (E) Sb-Al-Al plane; (F) Al-Al-Al plane.

CDD is another analytical tool on bonding characteristic. CDD shows the electron density difference between compounds and their corresponding single atom. As pointed out by Krba *et al.*[38], covalently bonded, ionically bonded and

metallic system show significant difference in CDD. For example, in crystal Si, the electron charge pileup(observed midway between the two Si atoms) is a signature of covalent bonding. Fig.5 shows CDD along different planes in a-AlSb model. The conclusions from the CDD are as the same as the ones from ELF: Al-Sb bonds display sp^3 type of covalent bonding. Al-Al bonds show metallic bonding as well as covalent bonding. According to the result of CDD and ELF analyses, amorphous AlSb mainly exhibits sp^3 type of covalent bonding. Al homopolar connection shows partial metallic bonding, and also interesting covalent bonding with highly localized electrons.

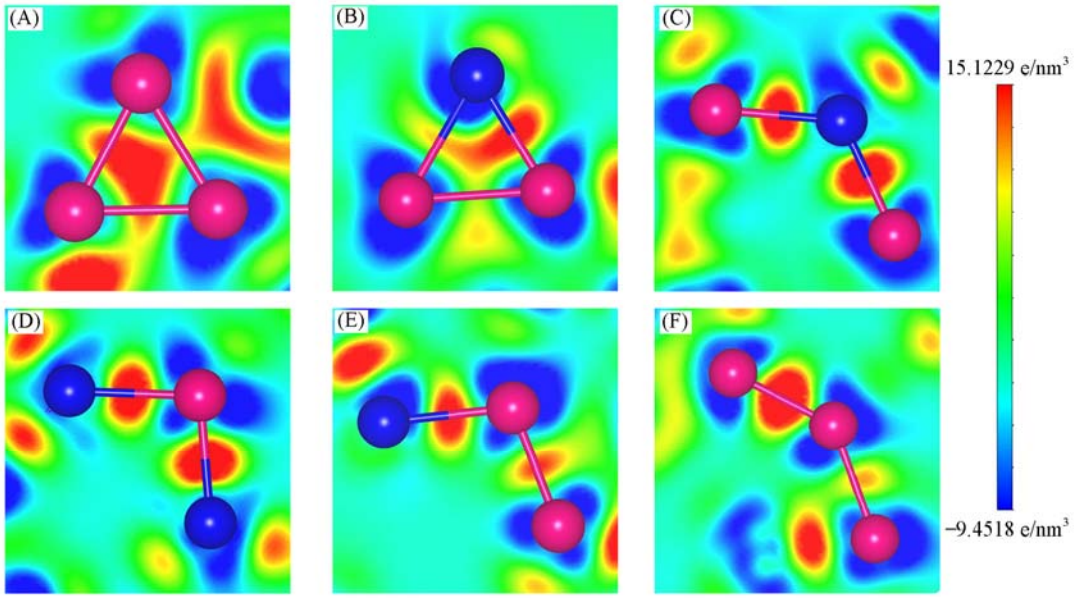

Fig.5 Charge density difference(CDD) along the plane of specific structures

(A) Al-Al-Al 3-fold ring; (B) Al-Sb-Al 3-fold ring; (C) Al-Sb-Al atom chain; (D) Sb-Al-Sb atom chain; (E) Al-Al-Sb atom chain; (F) Al-Al-Al atom chain.

4 Conclusions

By AIMD simulation, we obtained the atomic picture of amorphous AlSb phase-change material. The basic sp^3 atomic network in the amorphous phase was observed, which is reflected by the main BAD around 109.5° and the main coordination number of 4. In addition, a BAD around 60° is also found due to Al accumulation in the form of triangular structure. Analyses of ELF and CDD show Al-Sb forms normal covalent bonding and Al-Al forms metallic bonding. An interesting covalent Al-Al bonding can also be observed. After a part of Al accumulation, we proposed that on the one hand the Sb-rich region in amorphous AlSb can retain the rapid crystallization like pure Sb solid and on the other hand the remaining Al atoms can stabilize Sb-rich network with the intrinsic sp^3 bonding characteristic. Thus, it is the reason why AlSb holds both good data retention(amorphous stability) and suitable crystallization speed. The present study offers a microscopic amorphous picture of AlSb alloy and the possible switching mechanism for phase change memory devices.

References

[1] Wuttig M., Yamada N., *Nat. Mater*., **2007**, *6*, 824

[2] Li X. B., Liu X. Q., Han X. D., Zhang S. B., *Phys. Status Solidi B*, **2012**, *249*, 1861

[3] Ovshinsky S. R., *Phys. Rev. Lett*., **1968**, *21*, 1450

[4] Lencer D., Salinga M. M., Wuttig M., *Adv. Mater.*, **2011**, *23*, 2030

[5] Hosseini M., Rebic S., Sparkes B. M., Teamley J., Buchler B. C., Lam P. K., *Light: Sci. Appl*., **2012**, *1*, e40

[6] Los J. H., Kühne T. D., Gabard S., Bernasconi M., *Phys. Rev. B*, **2013**, *88*, 174203

[7] Zhu M., Xia M. J., Rao F., Li X. B., Wu L. C., Ji X. L., Lü S. L., Song Z. T., Feng S. L., Sun H. B., Zhang S. B., *Nat. Commun*., **2014**, *5*, 4086

[8] Wang X. P., Chen N. K., Li X. B., Cheng Y., Liu X. Q., Xia M. J., Song Z. T., Han X. D., Zhang S. B., Sun H. B., *Phys. Chem. Chem. Phys*., **2014**, *16*, 10810

[9] Yamada N., Ohno E., Nishiuchi K., Akahira N., Takao M., *J. Appl. Phys*., **1991**, *69*, 2849

[10] Alola J., Larrucea J., Jones R. O., *Phys. Rev. B*, **2011**, *83*, 094113

[11] Maeda T., Terao M., Shimano T., *Jpn. J. Appl. Phys*., **2003**, *42*, 1044

[12] Xiang C. Y., Koo W., So F., Sasabe H., Kido J., *Light: Sci. Appl*., **2013**, *2*, e80

[13] Chen N. K., Li X. B., Wang X. P., Xia M. J., Xie S. Y., Wang H. Y., Song Z. T., Zhang S. B., Sun H. B., *Acta Mater.*, **2015**, *90*, 88

[14] Cabral C., Krusin-Elbaum L., Bruley J., Raoux S., Deline V., Madan A., Pinto T., *Appl. Phys. Lett.*, **2008**, *93*, 071906

[15] van Pieterson L., van Schijndel M., Rijpers J. C. N., Kaiser M., *Appl. Phys. Lett.*, **2003**, *83*, 1373

[16] Callan J. P., Kim A. M. T., Roeser C. A. D., Mazur E., *Phys. Rev. Lett.*, **2001**, *86*, 3650

[17] Zhang T., Song Z. T., Wang F., Liu B., Feng S. L., Chen B., *Appl. Phys. Lett.*, **2007**, *91*, 222102

[18] Zhou X. L., Wu L. C., Song Z. T., Rao F., Ren K., Peng C., Song S. N., Liu B., Feng S. L., *Appl. Phys. Lett.*, **2013**, *103*, 072114

[19] Liu X. Q., Li X. B., Zhang L., Cheng Y. Q., Yan Z. G., Xu M., Han X. D., Zhang S. B., Zhang Z., Ma E., *Phys. Rev. Lett.*, **2011**, *106*, 025501

[20] Kolobov A. V., Fons P., Frenkel A. I., Ankudinov A. L., Tominaga J.,

Uruga T., *Nat. Mater.*, **2004**, *3*, 703
[21] Li X. B., Liu X. Q., Liu X., Han D., Zhang Z., Han X. D., Sun H. B., Zhang S. B., *Phys. Rev. Lett.*, **2011**, *107*, 015501
[22] Shportko K., Kremers S., Woda M., Lencer D., Roberson J., Wuttig M., *Nat. Mater.*, **2008**, *7*, 653
[23] Kohn W., Sham L. J., *Phys. Rev.*, **1965**, *140*, A1133
[24] Hohenberg P., Kohn W., *Phys. Rev.*, **1964**, *136*, B86
[25] Kresse G., Furthmüller J., *Phys. Rev. B*, **1996**, *54*, 11169
[26] Zhao H., Zhou L., Wei D. S., Zhou X. J., Shi H. F., *Chem. J. Chinese Universities*, **2014**, *35*(8), 1731
[27] Blöchl P. E., *Phys. Rev. B*, **1994**, *50*, 17953
[28] Han D., West D., Li X. B., Xie S. Y., Sun H. B., Zhang S. B., *Phys. Rev. B*, **2010**, *82*, 155132
[29] Perdew J. P. Wang Y., *Phys. Rev. B*, **1986**, *33*, 8800
[30] Perdew J. P., Burke K., Ernzerhof M., *Phys. Rev. Lett.*, **1996**, *77*, 3865
[31] Blunt R. F., Frederikse H. P. R., Becker J. H., Hosler W. R., *Phys. Rev.*, **1954**, *96*, 578
[32] Herczog A., Haberecht R. R., Middleton A. E., *J. Electrochem. Soc.*, **1958**, *105*, 533
[33] Wang Y., Zhang X. C., Zhao L. J., Zhao X. X., Shi B. P., Fan C. M., *Chem. J. Chinese Universities*, **2014**, *35*(12), 2624
[34] Pyykkö P., Atsumi M., *Chem. Eur. J.*, **2009**, *15*, 186
[35] Xu M., Cheng Y. Q., Sheng H. W., Ma E., *Phys. Rev. B*, **2009**, *103*, 195502
[36] Kalikka J., Akola J., Jones R. O., *J. Phys: Condens. Matter.*, **2013**, *25*, 115801
[37] Savin A., Jepsen O., Flad J., Andersen O. K., Preuss H., von Schnering H. G., *Angew. Chem. Int. Ed. Engl.*, **1992**, *30*, 187
[38] Krba M., Kolobov A. V., Fons P., Tominaga J., Elliott S. R., Hegedus J., Uruga T., *Phys. Rev. B*, **2011**, *83*, 054203